Supporting Material

for "Allosteric Effects of Sodium Ion Binding on Activation of the M3 Muscarinic G-Protein Coupled Receptor" by Yinglong Miao, Alisha D Caliman and J. Andrew McCammon.

System Setup

Simulations of the M3 muscarinic receptor were carried out using the inactive tiotropium(antagonist)-bound X-ray structure (PDB: 4DAJ) that was determined at 3.40 Å resolution(1). Preparation of the M3 model system follows a similar procedure as previously used for the M2 receptor(2). To simulate the apo form of the M3 receptor, tiotropium was removed from the ligand-binding site. The T4 lysozyme that was fused into the protein to replace intracellular loop 3 (ICL3) for crystallizing the receptor was omitted from all simulations, based on previous findings that removal of the bulk of ICL3 does not appear to affect GPCR function and ICL3 is highly flexible(3). All chain termini were capped with neutral groups (acetyl and methylamide). Two disulphide bonds that were resolved in the crystal structure, *i.e.*, C3.25-$C220^{ECL2}$ and C6.61-C7.29, were maintained in the simulations. Using the *psfgen* plugin in VMD(4), the D2.50 residue was either deprotonated or protonated to investigate the allosteric effects of sodium ion binding to the M3 receptor. All other protein residues were set to the standard CHARMM protonation states at neutral pH(5), including the deprotonated D3.32 residue in the orthosteric site.

The M3 receptor was inserted into a palmitoyl-oleoyl-phosphatidyl-choline (POPC) bilayer with all overlapping lipid molecules removed using the *Membrane* plugin in VMD(4). The system charges were then neutralized either at 0.15 M NaCl concentration or only 14 Cl^- ions for simulating the D2.50-protonated system in the absence of Na^+ using the *Solvate* plugin in VMD(4). The simulation systems of the M3 receptor initially measured about 80 × 87 × 97 $Å^3$ with 130 lipid molecules, ~11,200 water molecules and a total of ~55,500 atoms. Periodic boundary conditions were applied on all simulation systems.

Molecular Dynamics Simulations

Molecular dynamics (MD) simulations were performed using NAMD2.9(6). The CHARMM27 parameter set with CMAP terms was used for the protein(7, 8), CHARMM36 for the POPC lipids(9), and TIP3P model for the water molecules(10). A cutoff distance of 12 Å was used for

the van der Waals and short-range electrostatic interactions and the long-range electrostatic interactions were computed with the particle-mesh Ewald summation method(11) using a grid point density of 1/Å. A 2 fs integration time-step was used for all MD simulations and a multiple-time-stepping algorithm(6) was employed with bonded and short-range nonbonded interactions computed every time-step and long-range electrostatic interactions every two time-steps. The SHAKE(12) algorithm was applied to all hydrogen-containing bonds.

Simulations of the M3 receptor started with equilibration of the lipid tails. With all other atoms fixed, the lipid tails were energy minimized for 1000 steps using the conjugate gradient algorithm and melted with an NVT run for 0.5 *ns* at 310 K. The two systems were further equilibrated using an NPT run at 1 atm and 310 K for 10 *ns* with 5 kcal/(mol·Å^2) harmonic position restraints applied to the crystallographically-identified atoms in the protein and ligand. The system volume was found to decrease with a flexible unit cell applied and level off during the second half of the 10 *ns* NPT run, suggesting that solvent and lipid molecules in the system were well equilibrated. Final equilibration of the two systems was performed using an NPT run at 1 atm and 310 K for 0.5 *ns* with all atoms unrestrained. After these minimization and equilibration procedures, production conventional MD (cMD) simulations were performed on the two systems for 100 *ns* at 1 atm pressure and 310 K with a constant ratio constraint applied on the lipid bilayer in the X-Y plane.

Accelerated Molecular Dynamics Simulations

With the accelerated MD (aMD) implemented in NAMD2.9(13), aMD simulations were performed on the M3 using the "dual-boost" version(14). Boost potential was applied to both dihedral angles and the total energy across all individual atoms with $E_{\text{dihed}} = V_{\text{dihed\_avg}} + 0.3*V_{\text{dihed\_avg}}$, $\alpha_{\text{dihed}} = 0.3*V_{\text{dihed\_avg}}/5$; $E_{\text{total}} = V_{\text{total\_avg}} + 0.2*N_{\text{atoms}}$ and $\alpha_{\text{total}} = 0.2*N_{\text{atoms}}$. Two independent 600 *ns* aMD runs were performed on the D2.50-deprotonated receptor by restarting from the final structure of the 100 *ns* cMD simulation with random atomic velocity initializations at 310 K, and similarly for five independent 600 *ns* aMD runs on the D2.50-protonated receptor in 0.15M NaCl solution. Three independent 600 *ns* aMD runs were also performed on the D2.50-protonated receptor in the absence of Na^+ (with only 14 Cl^- ions added to neutralize the system charge) for comparison. The cMD and aMD simulations that were performed on the M3 receptor are summarized in **Table 1**.

Table S1 The shortest distance (D_0) and number of suboptimal paths (N_{sop}) obtained from network analysis of the (a) D2.50-deprotonated and D2.50-protonated M3 receptor between key residues in the extracellular vestibule and orthosteric ligand-binding site (N6.58, W7.35, W6.48 and N6.52) and those in the intracellular G-protein coupling site (E6.30, Y5.58 and Y7.53). The N_{sop} values that were calculated within a distance limit δ=20 of the shortest paths are listed. Overall, the D2.50-protonated receptor shows decreased distances and increased number of suboptimal paths for signaling compared with the D2.50-deprotonated receptor.

D_0 (N_{sop})		Extracellular		Orthosteric Site	
		N6.58	W7.35	W6.48	N6.52
Intracellular	E6.30	211 (36)	251 (36)	178 (8)	187 (10)
	Y5.58	287 (79)	293 (80)	244 (45)	263 (45)
	Y7.53	171 (47)	115 (7)	176 (4)	180 (31)

(a) D2.50-protonated / 0.15 M Na^+

D_0 (N_{sop})		Extracellular		Orthosteric Site	
		N6.58	W7.35	W6.48	N6.52
Intracellular	E6.30	284 (29)	255 (27)	230 (3)	255 (6)
	Y5.58	277 (21)	352 (35)	270 (8)	248 (7)
	Y7.53	237 (31)	188 (8)	194 (3)	208 (4)

(b) D2.50-deprotonated / 0.15 M Na^+

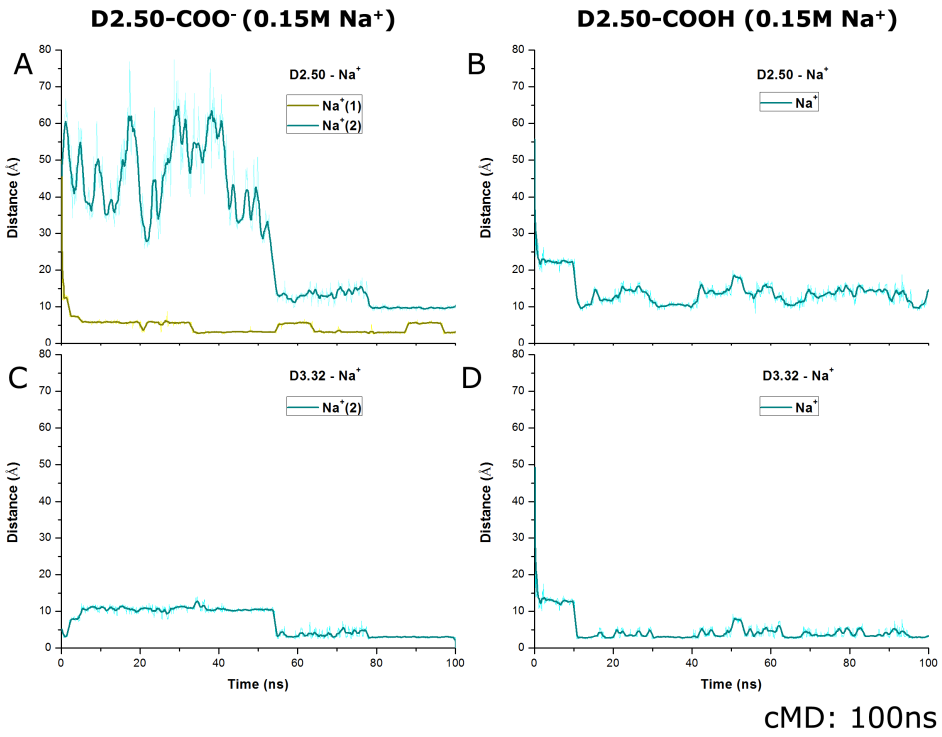

Figure S1 Timecourses of sodium ion binding to the M3 receptor: In an initial 100 *ns* cMD simulation of the D2.50-deprotonated receptor, a sodium ion (yellow) enters the orthosteric site and then binds to the D2.50 allosteric site, followed by a second sodium ion (cyan) binding to the D3.32 orthosteric site. (A) The distances of the two sodium ions to the D2.50 C_γ atom decrease from >40 Å to ~3 Å and ~10 Å, respectively, and (C) the distance of the second sodium ion to the D3.32 C_γ atom decreases to ~3 Å at the end of the cMD simulation. In another 100 *ns* cMD simulation of the D2.50-protonated receptor, no sodium ion binds to the D2.50 allosteric site but one binds to the D3.32 orthosteric site. Distance of the sodium ion to the C_γ atoms of D2.50 and D3.32 are plotted in (B) and (D), respectively.

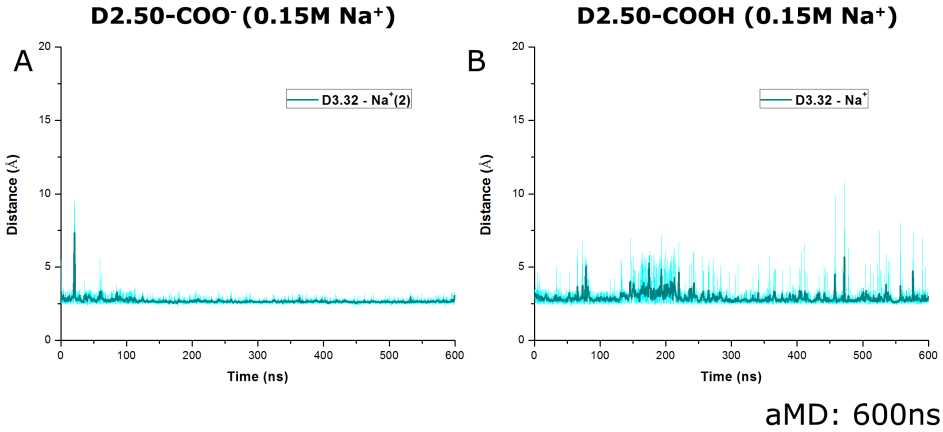

Figure S2 A sodium ion is bound to the deprotonated D3.32 residue in both the (A) D2.50-deprotonated and (B) D2.50-protonated M3 receptor in 0.15M Na^+ solution.

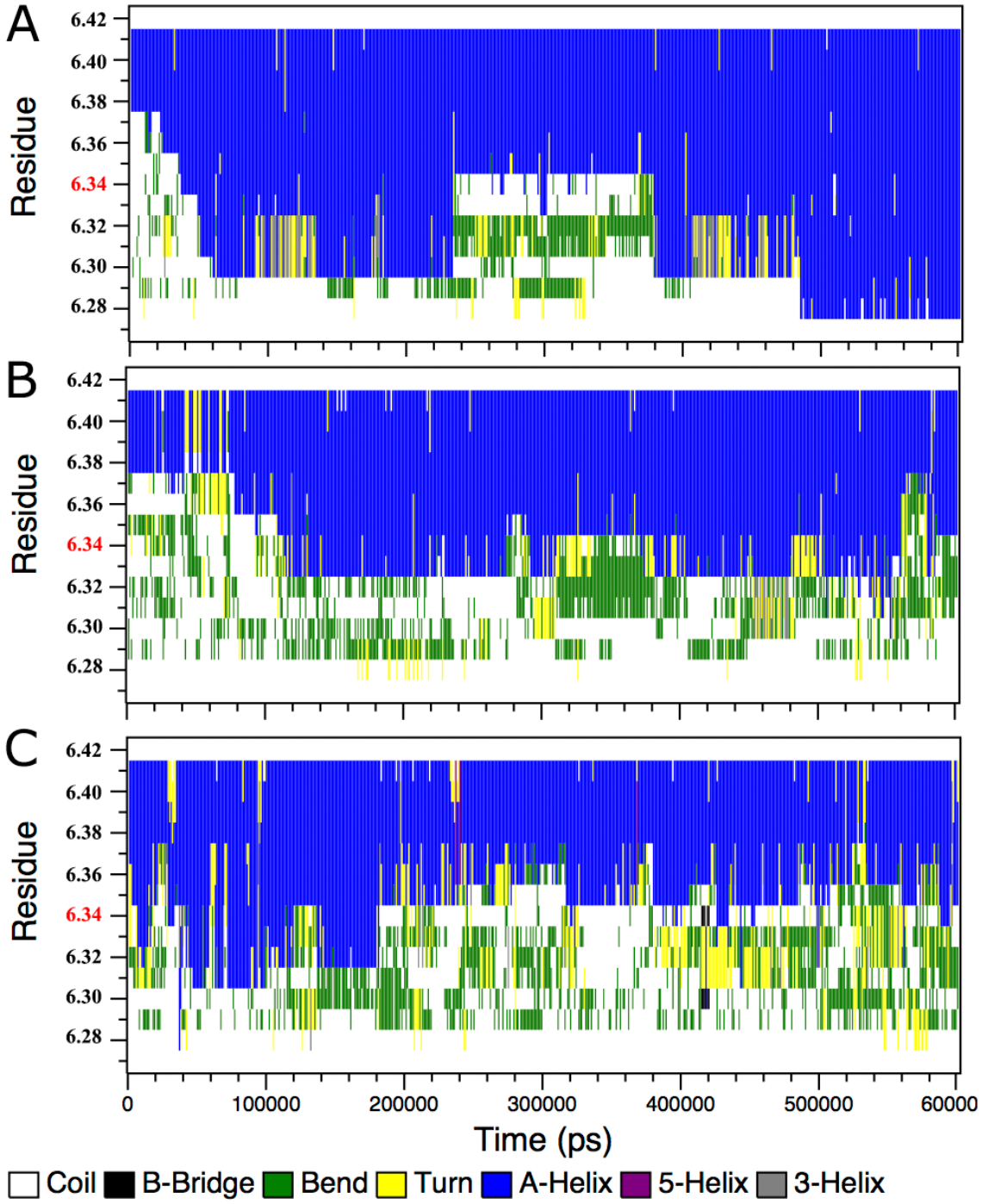

Figure S3 Time evolution of the secondary structure of the TM6 intracellular region, which has three residues K6.31−A6.33 missing and exhibits random coil in the starting X-ray structure, during representative 600 *ns* aMD simulations of (A) D2.50-COO^- / 0.15M Na^+, (B) D2.50-COOH / 0.15M Na^+ and (C) D2.50-COOH / No Na^+. In **Figure 1**, the R3.50-A6.34 distance is reported only when helical structure is formed for at least residues 6.42 to 6.33 in this region.

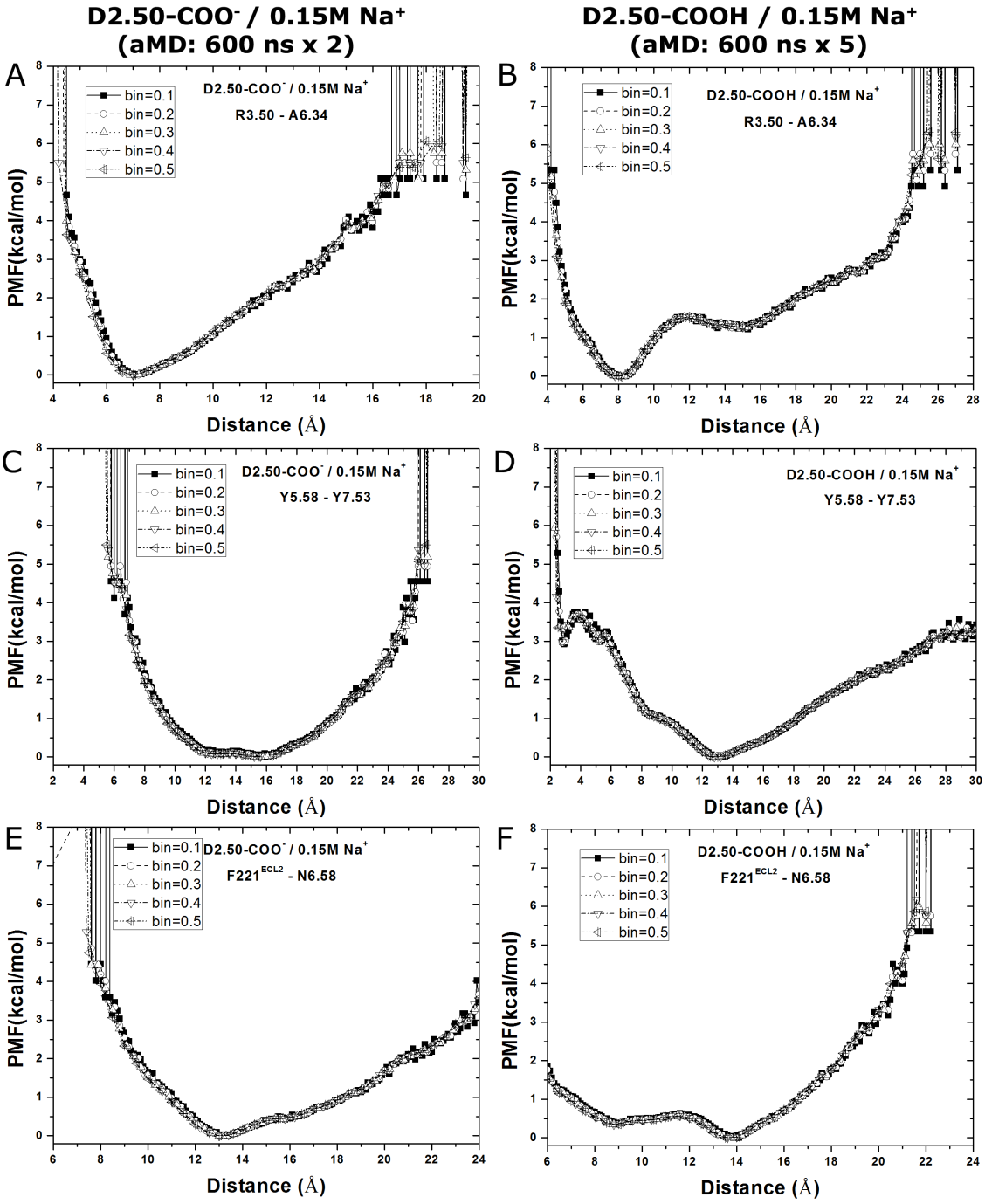

Figure S4 The potential of mean force (PMF) calculated from aMD simulations of the D2.50-deprotonated and D2.50-protonated M3 receptor for the distances between (A-B) R3.50-A6.34, (C-D) Y5.58-Y7.53 and (E-F) $F221^{ECL2}$-N6.58. The two and five independent 600 *ns* aMD runs are combined for the PMF calculations on the D2.50-deprotonated and D2.50-protonated systems, respectively. Note that because aMD suffers from large energetic noise for reweighting in the M3 receptor simulations(15), PMF profiles computed without reweighting are presented here.

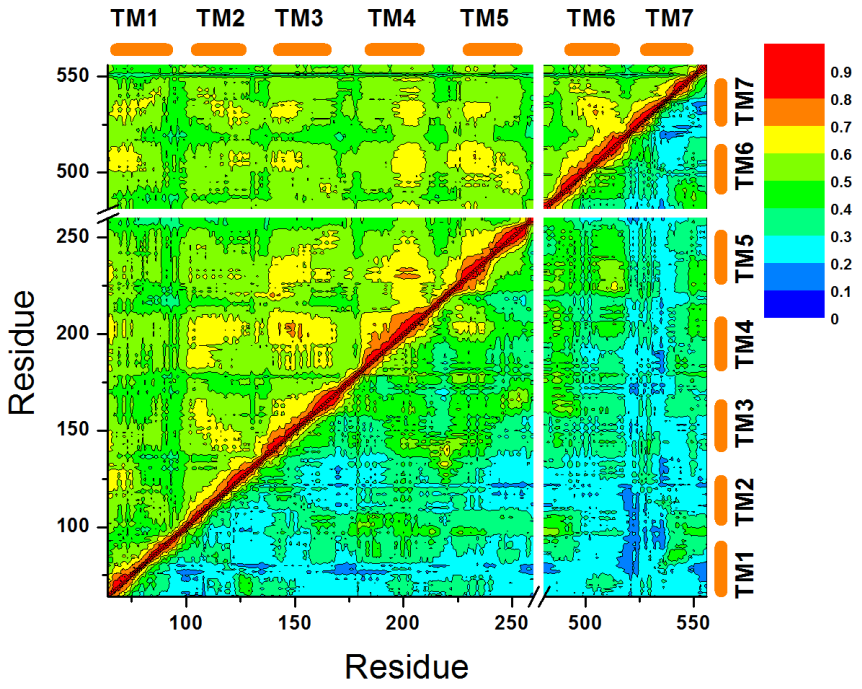

Figure S5 Generalized cross correlations calculated for residue motions in aMD simulations of the M3 receptor: the D2.50-deprotonated system in 0.15M Na^+ solution (lower triangle) compared with the D2.50-protonated system without Na^+. Orange bars on the top and right axes denote the seven transmembrane helices (TM1 to TM7).

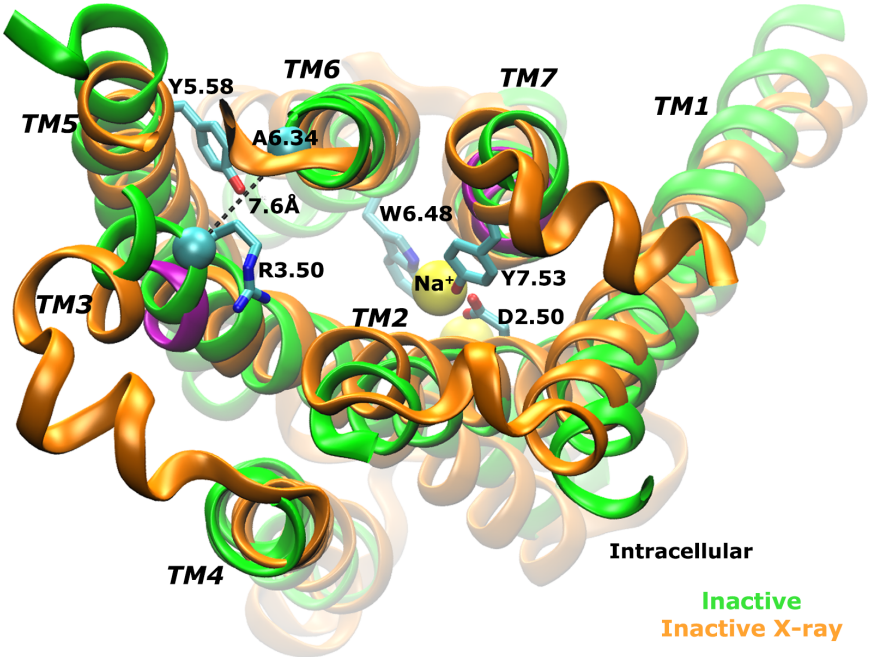

Figure S6 An inactive conformation of the D2.50-deprotonated M3 receptor that reorients the Y5.58 side chain from the lipid-exposed surface in the X-ray structure to the interface between the TM5 and TM6 helices. Formation of α helical structure is also found in the TM6 intracellular region.

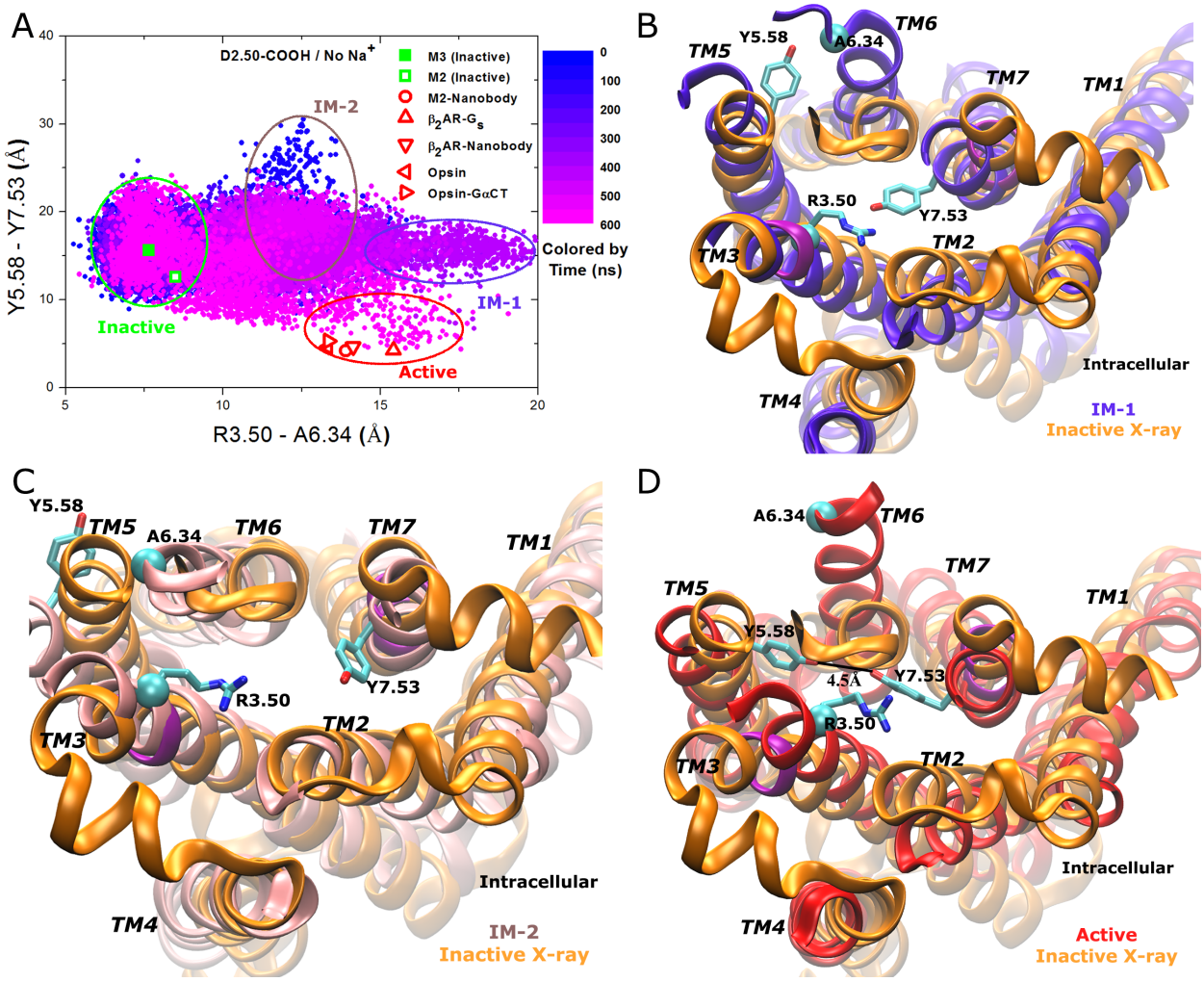

Figure S7 (A) Conformational space sampled by the D2.50-protonated M3 receptor in the absence of Na^+. Related GPCR X-ray structures are marked similarly as in **Figure 3A**. The intracellular view of different conformers of the M3 receptor compared with the X-ray structure (orange): (B) "IM-1" intermediate (blue), (C) "IM-2" intermediate (pink) and (D) active (red).

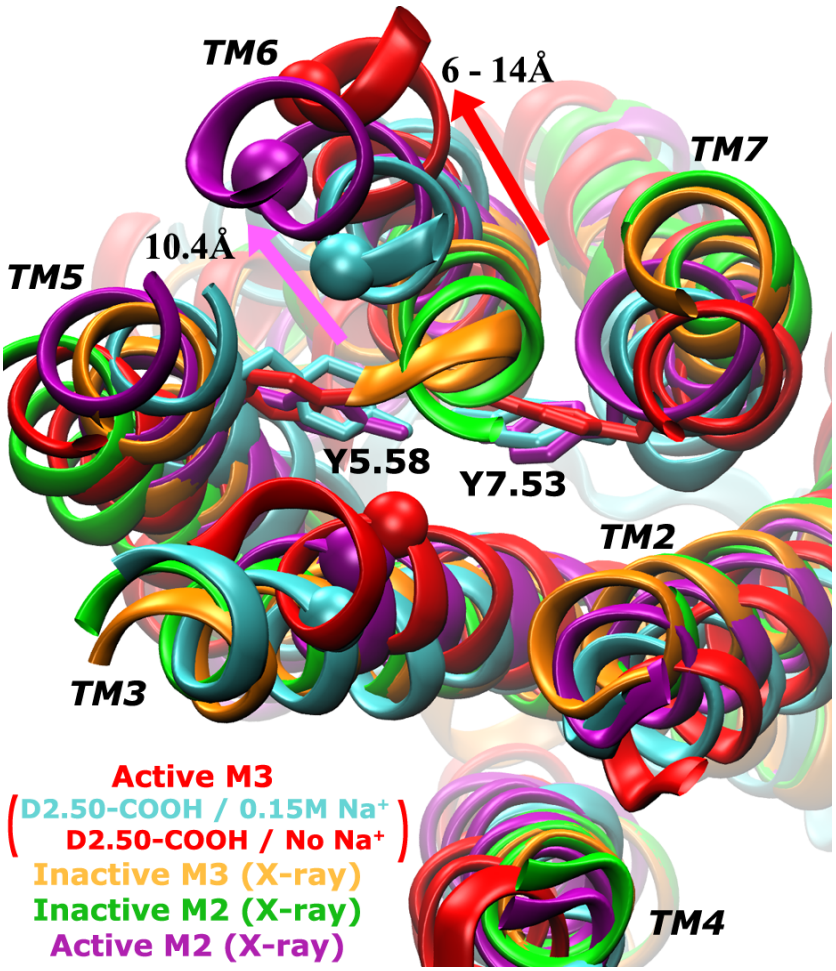

Figure S8 Comparison of the representative active conformations of the D2.50-protonated M3 receptor observed in 0.15M Na^+ solution (red) and without Na^+ (cyan) with the active M2 X-ray structure (purple, 4MQS), along with the inactive M3 (orange, 4DAJ) and M2 (green, 3UON) X-ray structures.

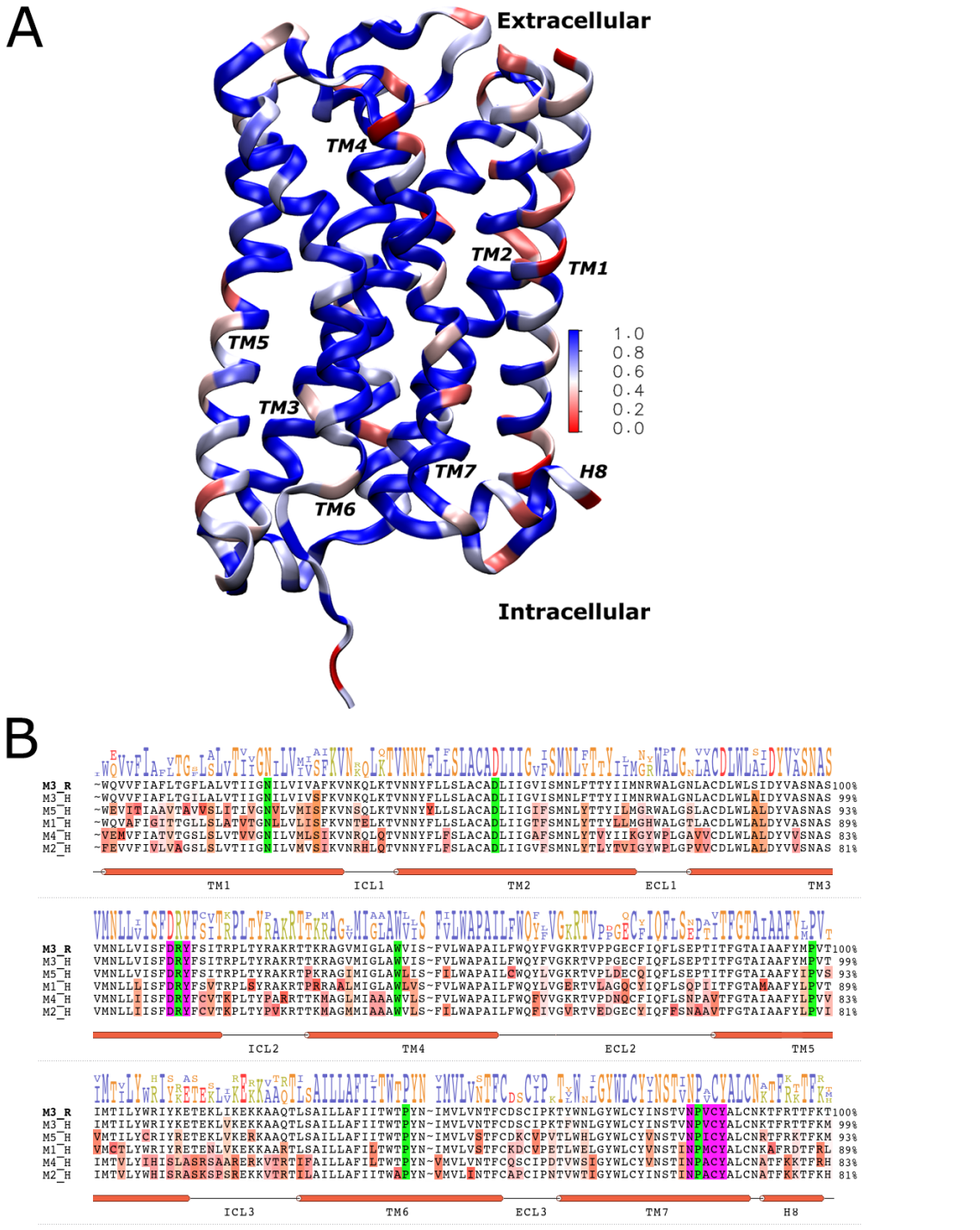

Figure S9 (A) Conservation of the protein primary sequence of the rat M3 muscarinic receptor (PDB: 4DAJ) in the five human muscarinic receptors. Blue means high conservation, while red means low conservation. (B) Sequence alignment of the rat M3 muscarinic receptor (M3_R) and five human muscarinic subtypes (M1_H to M5_H) sorted by the sequence similarity to M3_R. Residues of the ICL3 bulk that were not determined in the 4DAJ X-ray structure are excluded for analysis here.

References

1. Haga, K., A. C. Kruse, H. Asada, T. Yurugi-Kobayashi, M. Shiroishi, C. Zhang, W. I. Weis, T. Okada, B. K. Kobilka, T. Haga, and T. Kobayashi. 2012. Structure of the human M2 muscarinic acetylcholine receptor bound to an antagonist. Nature 482:547-551.
2. Miao, Y., S. E. Nichols, P. M. Gasper, V. T. Metzger, and J. A. McCammon. 2013. Activation and dynamic network of the M2 muscarinic receptor. Proc. Natl. Acad. Sci. U. S. A. 110:10982-10987.
3. Dror, R. O., D. H. Arlow, P. Maragakis, T. J. Mildorf, A. C. Pan, H. Xu, D. W. Borhani, and D. E. Shaw. 2011. Activation mechanism of the β2-adrenergic receptor. Proc. Natl. Acad. Sci. U. S. A. 108:18684-18689.
4. Humphrey, W., A. Dalke, and K. Schulten. 1996. VMD: Visual molecular dynamics. J Mol Graph Model 14:33-38.
5. Kruse, A. C., J. Hu, A. C. Pan, D. H. Arlow, D. M. Rosenbaum, E. Rosemond, H. F. Green, T. Liu, P. S. Chae, R. O. Dror, D. E. Shaw, W. I. Weis, J. Wess, and B. K. Kobilka. 2012. Structure and dynamics of the M3 muscarinic acetylcholine receptor. Nature 482:552-556.
6. Phillips, J. C., R. Braun, W. Wang, J. Gumbart, E. Tajkhorshid, E. Villa, C. Chipot, R. D. Skeel, L. Kale, and K. Schulten. 2005. Scalable molecular dynamics with NAMD. J. Comput. Chem.:1781-1802.
7. MacKerell, A. D., D. Bashford, M. Bellott, R. L. Dunbrack, J. D. Evanseck, M. J. Field, S. Fischer, J. Gao, H. Guo, S. Ha, D. Joseph-McCarthy, L. Kuchnir, K. Kuczera, F. T. K. Lau, C. Mattos, S. Michnick, T. Ngo, D. T. Nguyen, B. Prodhom, W. E. Reiher, B. Roux, M. Schlenkrich, J. C. Smith, R. Stote, J. Straub, M. Watanabe, J. Wiorkiewicz-Kuczera, D. Yin, and M. Karplus. 1998. All-Atom Empirical Potential for Molecular Modeling and Dynamics Studies of Proteins. J. Phys. Chem. B 102:3586-3616.
8. MacKerell, A. D., Jr., M. Feig, and C. L. Brooks, 3rd. 2004. Improved treatment of the protein backbone in empirical force fields. J Am Chem Soc 126:698-699.
9. Klauda, J. B., R. M. Venable, J. A. Freites, J. W. O'Connor, D. J. Tobias, C. Mondragon-Ramirez, I. Vorobyov, A. D. MacKerell, and R. W. Pastor. 2010. Update of the CHARMM All-Atom Additive Force Field for Lipids: Validation on Six Lipid Types. The Journal of Physical Chemistry B 114:7830-7843.
10. Jorgensen, W. L., J. Chandrasekhar, J. D. Madura, R. W. Impey, and M. L. Klein. 1983. Comparison of Simple Potential Functions for Simulating Liquid Water. J. Chem. Phys. 79:926-935.
11. Essmann, U., L. Perera, M. L. Berkowitz, T. Darden, H. Lee, and L. G. Pedersen. 1995. A Smooth Particle Mesh Ewald Method. J. Chem. Phys. 103:8577-8593.
12. Ryckaert, J.-P., G. Ciccotti, and H. J. C. Berendsen. 1977. Numerical integration of the cartesian equations of motion of a system with constraints: molecular dynamics of n-alkanes. J. Comput. Phys. 23:327-341.
13. Wang, Y., C. B. Harrison, K. Schulten, and J. A. McCammon. 2011. Implementation of Accelerated Molecular Dynamics in NAMD. Comput. Sci. Discov. 4:015002.
14. Hamelberg, D., C. A. F. de Oliveira, and J. A. McCammon. 2007. Sampling of slow diffusive conformational transitions with accelerated molecular dynamics. J. Chem. Phys. 127:155102.
15. Miao, Y., S. E. Nichols, and J. A. McCammon. 2014. Free Energy Landscape of G-Protein Coupled Receptors, Explored by Accelerated Molecular Dynamics. Phys. Chem. Chem. Phys. 16:6398 - 6406.